Journal of Power Sources 232 (2013) 234–239

Contents lists available at SciVerse ScienceDirect

Journal of Power Sources

journal homepage: www.elsevier.com/locate/jpowsour

Preparation of high performance carbon-coated $LiMnPO_4$ nanocomposite by an acetate-assisted antisolvent precipitation method

Kai Su, Feng Liu*, Jitao Chen*

Beijing National Laboratory for Molecular Sciences, Key Laboratory of Bioorganic Chemistry and Molecular Engineering of Ministry of Education, College of Chemistry and Molecular Engineering, Peking University, Beijing 100871, China

HIGHLIGHTS

- A novel antisolvent precipitation method is developed to synthesize $LiMnPO_4$ material.
- The precursor is composed of $Mn_3(PO_4)_2$ and Li_3PO_4 nanoparticles.
- The carbon-coated $LiMnPO_4$ with the particle size of 60 nm is obtained.
- The C-$LiMnPO_4$ material exhibits excellent rate capability and stable cyclability.

ARTICLE INFO

Article history:
Received 31 October 2012
Received in revised form
31 December 2012
Accepted 9 January 2013
Available online 18 January 2013

Keywords:
Lithium-ion battery
Lithium manganese phosphate
Antisolvent precipitation
Nanocomposite
Cathode material
Rate capability

ABSTRACT

A novel acetate-assisted antisolvent precipitation method combined with ball milling and heat treatment is developed to synthesize nanosized carbon-coated $LiMnPO_4$ material. The precursor prepared by the precipitation process is composed of $Mn_3(PO_4)_2$ and Li_3PO_4 nanoparticles. After heat treatment of the ball-milled mixture of precursor and glucose, the carbon-coated $LiMnPO_4$ with the particle size of around 60 nm is obtained. The $LiMnPO_4$ nanocomposite synthesized at the optimized conditions delivers specific discharge capacities of 154, 134, 120, 90, and 61 mAh g^{-1} at the rates of 0.05, 0.2, 1, 5, and 10C, respectively, which are comparable to some of the best reported C-$LiMnPO_4$ materials prepared by other synthesis methods. This material further exhibits good cycling stability, especially at high discharge rates of 5C and 10C.

1. Introduction

Lithium-ion batteries as the front-runners in energy storage systems have attracted much attention due to the growing market demand for portable electronic devices and electric vehicles [1–3]. In 1997, Padhi et al. introduced olivine-type lithium transition metal phosphates $LiMPO_4$ (M = Fe, Mn, Co, Ni) as desirable cathode materials owing to their outstanding properties such as high stability, environmental benignity, and low cost [4]. Among them, $LiFePO_4$ has been extensively studied and successfully commercialized [5–8]. Given the great success of $LiFePO_4$, $LiMPO_4$ (M = Mn, Co, Ni) with a higher redox potential is favored in the recent research. The high voltages of $LiCoPO_4$ (4.9 V vs. Li^+/Li) and $LiNiPO_4$ (5.1 V vs. Li^+/Li) materials are beyond the stable electrochemical windows of present electrolytes, thus developing $LiMnPO_4$ (4.1 V vs. Li^+/Li) seems to be more promising.

However, the inherently low ionic and electronic conductivities of $LiMnPO_4$ render it difficult to achieve excellent electrochemical activity [9]. Inspired by the previous research on $LiFePO_4$, the strategies including carbon coating [10], ion-doping [11], and particle size reduction [12,13] have been adopted to overcome these limitations. Various methods such as sol–gel [12], polyol [14], hydrothermal [15], solvothermal [16], ultrasonic spray pyrolysis [17], and precipitation [18–22] have already been attempted to prepare nanosized carbon-coated $LiMnPO_4$ (referred to as C-$LiMnPO_4$ hereafter). Of the reported methods, the precipitation process is

* Corresponding authors. Tel.: +86 10 62761187; fax: +86 10 62751708.
E-mail addresses: liufeng@pku.edu.cn (F. Liu), chenjitao@pku.edu.cn (J. Chen).

0378-7753/$ – see front matter © 2013 Elsevier B.V. All rights reserved.
http://dx.doi.org/10.1016/j.jpowsour.2013.01.054

a commercially viable one due to its simplicity and low cost. Delacourt et al. synthesized ~100 nm $LiMnPO_4$ particles by a direct precipitation technique [18]. Liu et al. used the 100–300 nm thick plate-like $NH_4MnPO_4 \cdot H_2O$ as the precursor to prepare $LiMnPO_4$ which preserved the morphology of $NH_4MnPO_4 \cdot H_2O$ [19]. Kim et al. synthesized 70 × 150 nm–100 × 300 nm $LiMnPO_4$ particles through a sequential precipitation [20]. In spite of these efforts, the $LiMnPO_4$ materials prepared by precipitation methods only exhibit moderate specific capacity and limited rate capability. Therefore, it is a great challenge to develop a new precipitation method to further decrease the particle size of the $LiMnPO_4$ material for improving its capacity, especially at high rates.

Antisolvent precipitation is a robust and scalable method mainly used in the preparation of nanoscale pharmaceutical ingredients [23–26]. According to classical precipitation theory, the formation mechanism of precipitate involves generation of supersaturation, nucleation, and particle growth. The kinetics of the latter two processes would determine the final size of precipitated particles. In an antisolvent precipitation process, the antisolvent is used to lower the solubility of compounds in the liquid solvent. Adding the solution of compounds to the antisolvent would generate the high supersaturation, which enables formation of nuclei more favorable than particle growth, yielding the precipitate with small particle size [23,24]. To our knowledge, antisolvent precipitation has not been used to prepare cathode materials. In the current efforts, we aim at developing a novel method based on antisolvent precipitation to synthesize ultrafine C-$LiMnPO_4$ composite.

Herein, we present an acetate-assisted antisolvent precipitation method combined with ball milling and heat treatment to synthesize C-$LiMnPO_4$ nanocomposite. The aqueous solution containing Mn^{2+} and PO_4^{3-} is added to the ethanol solution of lithium acetate for the preparation of the nanosized precipitate as the precursor. Ethanol serves as the antisolvent. Subsequently, the precursor is ball-milled with glucose and heat-treated to obtain C-$LiMnPO_4$. The compositions and morphologies of the precursor and $LiMnPO_4$ samples are studied by scanning electron microscopy, energy dispersive X-ray spectroscopy, and transmission electron microscopy. The synthetic conditions of C-$LiMnPO_4$ such as heating temperature, heating time, and glucose content are optimized. The C-$LiMnPO_4$ nanocomposite prepared by this method displays excellent rate capability and stable cycling performance.

2. Experimental

2.1. Reagents

Lithium acetate dihydrate ($LiAc \cdot 2H_2O$) and glucose were purchased from Beijing Yili Fine Chemical Company (Beijing, China). Manganese acetate tetrahydrate ($Mn(Ac)_2 \cdot 4H_2O$) was obtained from Xilong Chemical Limited Company (Shantou, China). H_3PO_4 (85 wt%), HCl (37 wt%), and anhydrous ethanol were purchased from Beijing Chemical Reagent Company (Beijing, China). All these reagents were of analytical grade and used as received without further purification.

2.2. Synthesis procedure

The aqueous solution was prepared by adding 14.7 g of $Mn(Ac)_2 \cdot 4H_2O$, 4.08 mL H_3PO_4, and 6 mL HCl to 50 mL deionized water. 600 mL ethanol acted as the antisolvent, in which 26.4 g of $LiAc \cdot 2H_2O$ was dissolved. The aqueous solution was dropped slowly to the ethanol solution at 70 °C under vigorous stirring, and then the mixture was kept at 70 °C for 3 h. The obtained white precipitate was washed several times with ethanol and dried in an oven at 60 °C for 4 h. Subsequently, the precipitate was ball-milled with or without glucose for 6 h and sintered at 550 °C for 5 h in N_2 atmosphere to prepare C-$LiMnPO_4$ and bare $LiMnPO_4$, respectively.

2.3. Characterization of morphology, structure, and composition

The crystal structures of bare $LiMnPO_4$ and C-$LiMnPO_4$ were identified by a D/max2400 power X-ray diffractometer (XRD) (Rigaka, Japan) with Cu-Kα radiation ($\lambda = 1.5405$ Å) in a 2θ range of 10°–70°. The morphologies of the prepared nanomaterials were observed with an S-4800 scanning electron microscope (SEM) (Hitachi, Tokyo, Japan) and a Tecnai G2 F20 transmission electron microscope (TEM) (FEI, Portland, USA). Energy dispersive X-ray spectroscope (EDS) was applied to analyze the elemental composition of the precipitate. Carbon contents of the composites were determined by a Vario EL III elemental analyzer (Elementar, Germany). An ASAP2010 apparatus (Micromeritics, USA) was employed to estimate the specific surface areas of bare $LiMnPO_4$ and C-$LiMnPO_4$ powders.

2.4. Electrochemical measurements

C-$LiMnPO_4$ (80 wt%), carbon black (10 wt%), and poly(vinylidene fluoride) binder (10 wt%) in *N*-methylpyrrolidone were stirred into a homogeneous slurry. The obtained mixture was casted on aluminum foil and dried under vacuum at 100 °C overnight. Round disks with a diameter of 12 mm were cut for electrochemical characterizations. The electrodes typically had an active material loading of 2.8 mg cm^{-2} and volumetric density of 1.1 g cm^{-3}. Coin-type cells were assembled in an argon-filled glove box ($O_2 \leq 50$ ppm, $H_2O \leq 0.1$ ppm). Lithium foil served as both anode and reference electrode. Mixture of ethylene carbonate and diethyl carbonate (1:1, *m*/*m*) containing 1 M $LiPF_6$ was used as the electrolyte. The cells were charged in a constant current and constant voltage mode (galvanostatically charged to 4.5 V at a rate of 0.05C, then potentiostatically charged at 4.5 V till current drops to 0.01C), and then discharged to 2.5 V at a specific rate (1C = 170 mAh g^{-1}) using a LAND battery test system. Cyclic voltammetry (CV) was operated on a CHI600D electrochemical workstation (Chenhua, Shanghai, China) between 2.5 V and 4.9 V at a scanning rate of 0.1 mV s^{-1}.

3. Results and discussion

3.1. Mechanism of the acetate-assisted antisolvent precipitation

The acetate-assisted antisolvent precipitation process for the preparation of the precursor is shown in Fig. 1. $Mn(Ac)_2$, H_3PO_4, and HCl are dissolved in deionized water to obtain a homogeneous aqueous solution. Then the aqueous solution is added to the ethanol solution of lithium acetate. Ethanol as the antisolvent induces the high supersaturation of Li_3PO_4 and $Mn_3(PO_4)_2$. Acetate in the ethanol as the proton acceptor further increases supersaturation while lithium ion acts as a precipitant to form Li_3PO_4. The high supersaturation created by acetate and antisolvent is supposed to lead a fast formation of nuclei and limited particle growth, yielding the precipitate with small particle size.

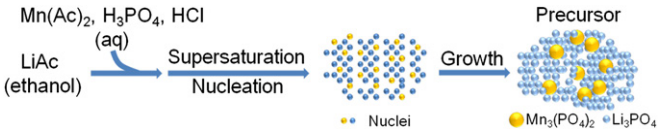

Fig. 1. Schematic illustration of the acetate-assisted antisolvent precipitation process.

3.2. Morphology and composition of the precursor

As illustrated in Fig. 2a, the precursor is composed of two kinds of particles: the nanospheres with 150–500 nm in diameter and the nanoparticles with the size of about 50 nm. The compositions of the nanospheres (Fig. 2b, inset) and the nanoparticles (Fig. 2c, inset) are studied by EDS. As shown in Table S1, the Mn/P ratio of the nanospheres is 1.52, which matches that of $Mn_3(PO_4)_2$. The Mn/P ratio of the nanoparticles is approximately equal to 0, indicating that the composition of these nanoparticles is Li_3PO_4. The precursor prepared by the newly developed precipitation method consists of $Mn_3(PO_4)_2$ nanospheres and Li_3PO_4 nanoparticles.

3.3. Effect of acidity of solution on purity of $LiMnPO_4$ sample

The acidity of solution has a strong impact on the composition of the precursor, and then affects the purity of $LiMnPO_4$ sample. We investigate the purities of $LiMnPO_4$ samples by adjusting the amount of HCl (n_{HCl}). These $LiMnPO_4$ samples are all obtained through heat treatment of the precursor at 550 °C for 5 h. Fig. 3 shows the XRD patterns of $LiMnPO_4$ samples prepared with various amounts of HCl. No obvious impurity appears when the amount of HCl is in the range of 65–88 mmol. Once the added amount of HCl reaches 96 mmol, $Mn_2P_2O_7$ is detected and the content of $Mn_2P_2O_7$ increases with the amount of HCl. This is because high acidity causes the formation of $Mn_7(PO_4)_4HPO_4$ (Supplementary Information, Fig. S1). The reaction between $Mn_7(PO_4)_4HPO_4$ and Li_3PO_4 during heat treatment produces $LiMnPO_4$ and $Mn_2P_2O_7$. It could be concluded that pure $LiMnPO_4$ compound would be obtained while the amount of HCl is controlled in the range of 65–88 mmol.

3.4. Effect of carbon coating on the particle growth in heat treatment

Generally, undesirable grain growth is accompanied with crystallization during the high temperature treatment. As particle size reduction is of significant importance for the improvement of electrochemical performance, particle growth should be suppressed. Carbon coating is recognized as an effective way to inhibit the particle growth during the sintering process [27].

Bare $LiMnPO_4$ is prepared through heat treatment of the precursor at 550 °C for 5 h. As shown in Fig. 4a, bare $LiMnPO_4$ is composed of nanoparticles with an average size of around 120 nm. TEM is applied to examine the crystallographic characteristic of bare $LiMnPO_4$. Fig. 4b shows clearly bare $LiMnPO_4$ has a high crystallinity. The atomic layers observed in the TEM image have a *d*-spacing value of 0.398 nm, corresponding to the (120) reflection of $LiMnPO_4$.

The C-$LiMnPO_4$ sample is also synthesized at the same heat treatment conditions. Prior to heat treatment, 20 wt% glucose as the carbon source is ball-milled with the precursor. Fig. 4e shows the XRD patterns of C-$LiMnPO_4$ and bare $LiMnPO_4$. All diffraction peaks could be indexed as olivine-type $LiMnPO_4$ with a *Pnmb* space group of the orthorhombic system (JCPDS No. 33-0804). No impurity phase is found. In comparison with $LiMnPO_4$, C-$LiMnPO_4$ has boarder XRD diffraction peaks, which suggest the crystallite size of C-$LiMnPO_4$ is smaller than that of $LiMnPO_4$. The SEM image of C-$LiMnPO_4$ is presented in Fig. 4c. The particle size of C-$LiMnPO_4$ is about 60 nm, much smaller than that of bare $LiMnPO_4$. The TEM image of C-$LiMnPO_4$ in Fig. 4d demonstrates that the surface of well-ordered $LiMnPO_4$ is uniformly covered by an amorphous carbon layer of 2 nm thick while the lattice fringe spacing (0.432 nm) is in coincidence with the (011) plane of $LiMnPO_4$. Apparently, the coated carbon layer inhibits the excessive growth of particles in the heating process. The specific surface areas of bare $LiMnPO_4$ and C-$LiMnPO_4$ are also investigated. The BET analysis (Supplementary Information, Fig. S2) reveals that the specific surface area of C-$LiMnPO_4$ (29.00 $m^2\ g^{-1}$) is larger than that of bare $LiMnPO_4$ (8.62 $m^2\ g^{-1}$), indicating the electrolyte is more accessible to the active material [28].

Cyclic voltammetry (CV) is a reliable predictor of the electrochemical performances of materials. The CV curves of bare $LiMnPO_4$ and C-$LiMnPO_4$ are shown in Fig. 5. No obvious peak is observed in the CV profile of bare $LiMnPO_4$. The negligible response suggests that bare $LiMnPO_4$ has a poor electrochemical performance. C-$LiMnPO_4$ exhibits a couple of obvious redox peaks at 3.89 V and 4.35 V, which are associated with reduction and oxidation of the Mn^{2+}/Mn^{3+} redox couple, respectively. In comparison with bare $LiMnPO_4$, the electrochemical activity of C-$LiMnPO_4$ is mainly

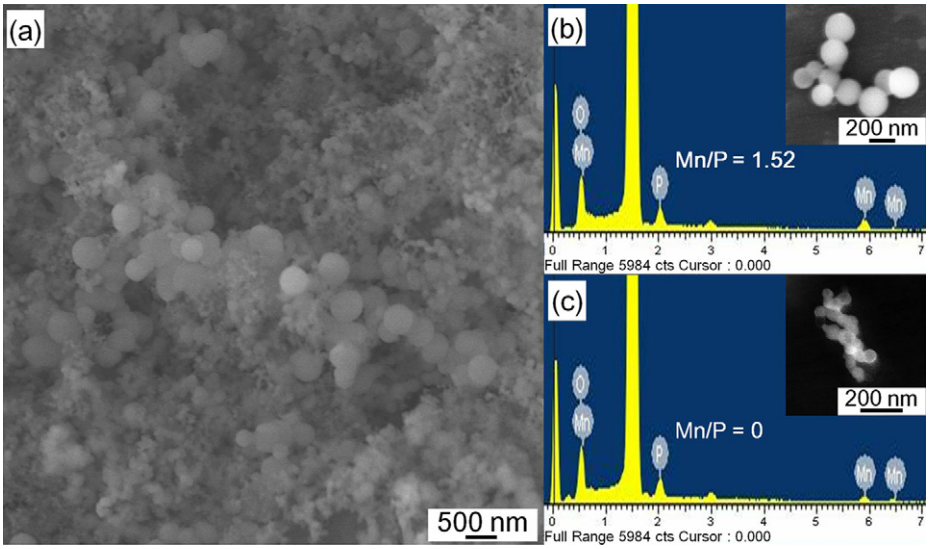

Fig. 2. (a) SEM image of the precursor. (b) SEM image of the separated nanospheres (inset) and the corresponding EDS map. (c) SEM image of the separated nanoparticles (inset) and the corresponding EDS map.

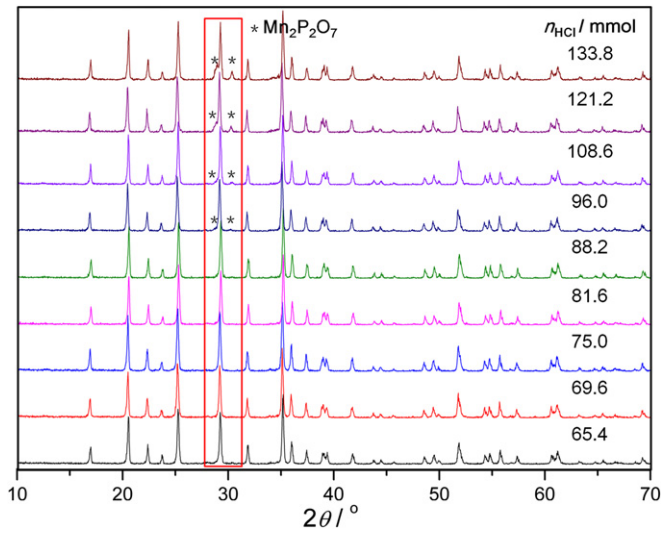

Fig. 3. XRD patterns of $LiMnPO_4$ samples prepared with various amounts of HCl. The $LiMnPO_4$ samples were synthesized at 550 °C for 5 h.

ascribed to the improvement of electronic conductivity (Table S2), smaller particle size, and higher specific surface area.

3.5. Optimization of synthetic conditions for C-$LiMnPO_4$

The conditions of heat treatment and carbon coating are systematically optimized to prepare C-$LiMnPO_4$ nanocomposite with high electrochemical performance. The discharge rate of all the samples is kept at 0.05C.

C-$LiMnPO_4$ composites are synthesized at various heating temperatures for 5 h with 20 wt% glucose. As shown in Fig. 6a, the initial specific discharge capacities of the samples obtained at 450, 500, 550, and 600 °C are 138, 147, 154, and 141 mAh g^{-1}, respectively. The C-$LiMnPO_4$ sample prepared at 550 °C has the highest discharge capacity. It could be clarified that lower heating temperature causes poor crystallinity (Supplementary Information, Fig. S3) [29], while higher heating temperature leads to the growth of crystallite (Supplementary Information, Table S3). Poor crystallinity and larger crystallite size both limit the specific discharge capacity of C-$LiMnPO_4$. The $LiMnPO_4$ sample prepared at 550 °C gives the best discharge capacity due to proper crystallinity and crystallite size.

Heating time is adjusted for the preparation of high performance C-$LiMnPO_4$ at 550 °C with 20 wt% glucose. Fig. 6b presents the initial discharge profiles of these samples prepared with various heating times. The specific discharge capacities of C-$LiMnPO_4$ heated for 2, 5, and 8 h are 152, 154, and 134 mAh g^{-1}, respectively. The sample synthesized by heat treatment for 5 h achieves the best performance. Here shorter heating time (2 h) has a negligible impact on the specific capacity, whereas longer heating time (8 h) causes larger grain size which has a negative impact on the capacity.

Different contents of glucose are used to synthesize C-$LiMnPO_4$ samples at 550 °C for 5 h. C-$LiMnPO_4$ prepared with 20 wt% glucose exhibits the highest discharge capacity, as shown in Fig. 6c. The residual carbon contents of C-$LiMnPO_4$ samples obtained with 10, 20, and 30 wt% glucose are 2.8, 5.7, and 6.5 wt%, respectively. The carbon coating layer on the surface of particles improves the electronic conductivity but hinders Li^+ diffusion [30]. The best result of the C-$LiMnPO_4$ sample synthesized with 20 wt% glucose is probably due to an optimal carbon coating thickness.

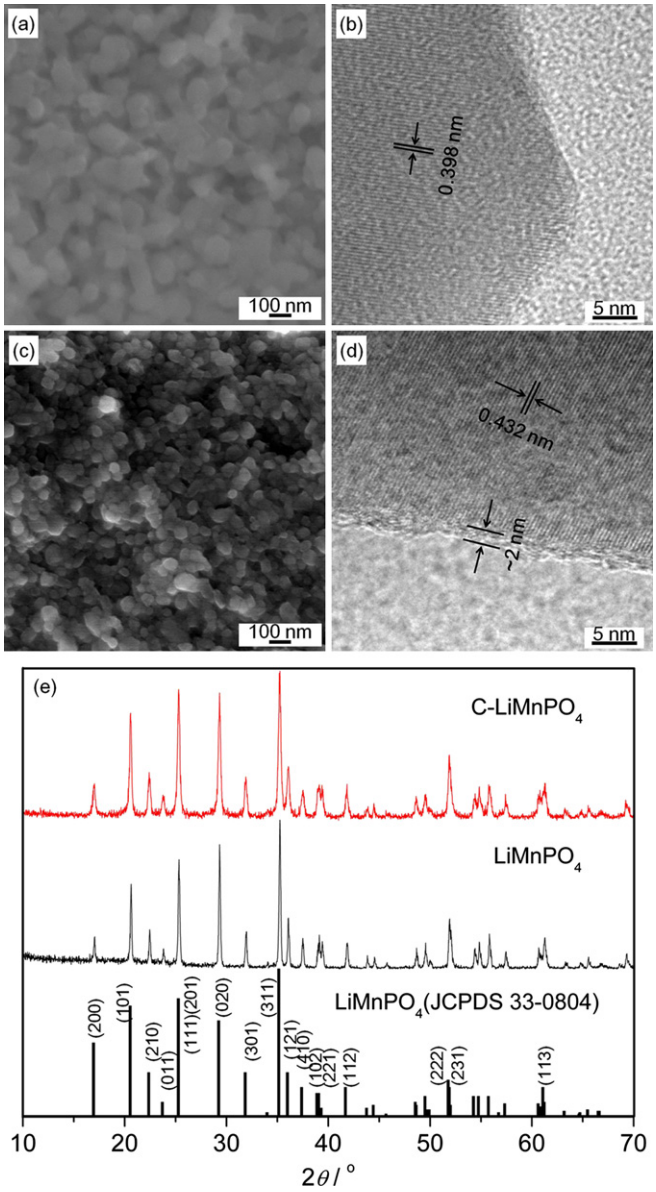

Fig. 4. SEM and TEM images of bare $LiMnPO_4$ (a, b) and C-$LiMnPO_4$ (c, d). XRD patterns of C-$LiMnPO_4$ and bare $LiMnPO_4$ (e). The samples were synthesized at 550 °C for 5 h.

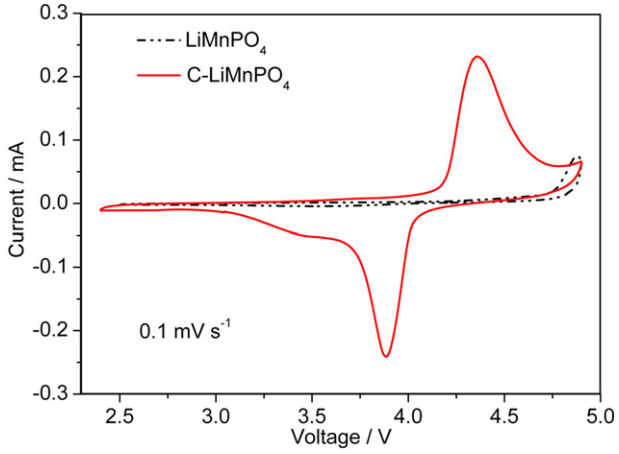

Fig. 5. Cyclic voltammograms of bare $LiMnPO_4$ and C-$LiMnPO_4$. The samples were synthesized at 550 °C for 5 h.

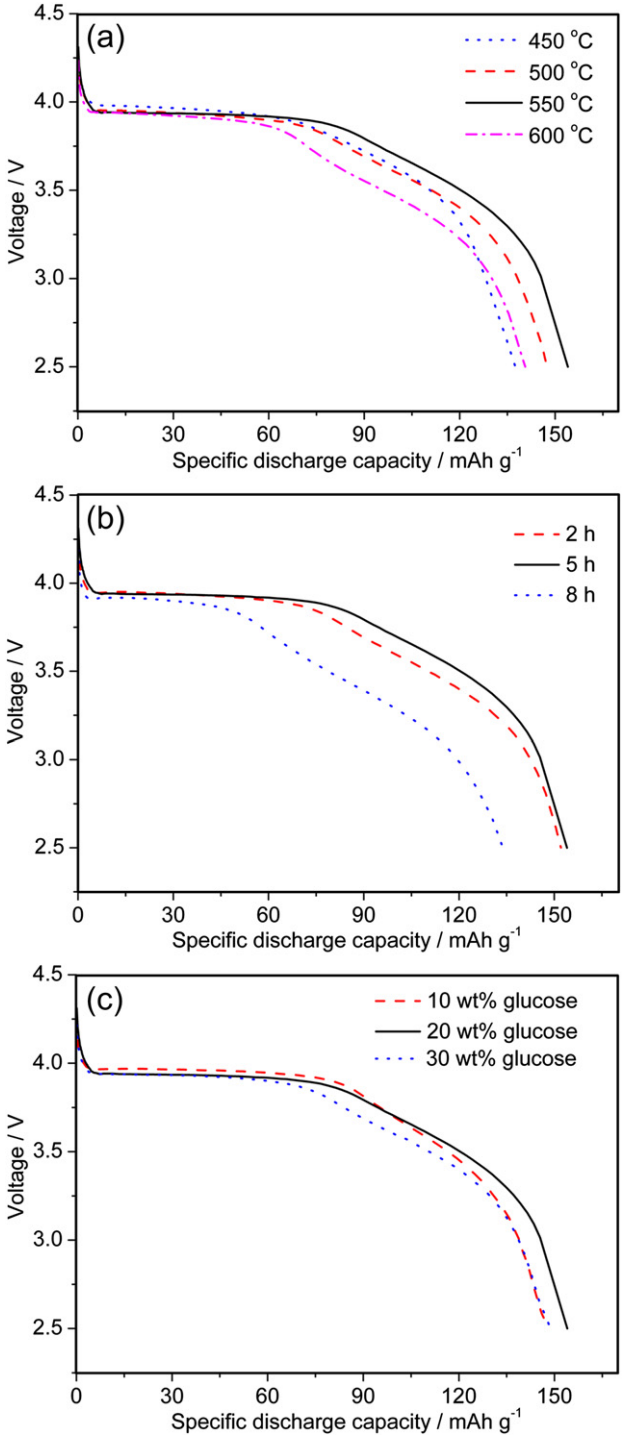

Fig. 6. Optimization of synthetic conditions for C-LiMnPO$_4$: (a) heating temperature, (b) heating time, and (c) the added amount of glucose. The discharge rate of all the samples was kept at 0.05C.

In summary, the optimal heating temperature, heating time, and glucose content are 550 °C, 5 h, and 20 wt%, respectively. The C-LiMnPO$_4$ sample is synthesized at these optimized conditions for the following electrochemical characterizations.

3.6. Electrochemical performance of C-LiMnPO$_4$

The rate capability of C-LiMnPO$_4$ is shown in Fig. 7a. The inset figure exhibits the corresponding discharge curves of C-LiMnPO$_4$ at various discharge rates. C-LiMnPO$_4$ nanocomposite delivers specific capacities of 154, 134, 120, 90, and 61 mAh g^{-1} at the discharge rates of 0.05, 0.2, 1, 5, and 10C, respectively. C-LiMnPO$_4$ displays an excellent rate performance especially at high discharge rates. When the discharge rate returns from 10C to 0.05C, the specific capacity is almost retrieved to that in the first third cycle of 0.05C. It suggests that high-rate cycling has little impact on capacity fade. Our material exhibits the highest rate performance among the LiMnPO$_4$ materials prepared by the precipitation methods [18–22]. The progress achieved here is ascribed to the smaller particle size which favors the capacity retention as the discharge rate increases. The rate capability of our C-LiMnPO$_4$ nanocomposite is also comparable to some of the best reported C-LiMnPO$_4$ materials prepared by other synthesis methods [12,14,17,31,32]. Furthermore, this simple precipitation method is more promising to be used in an industrial process due to low cost.

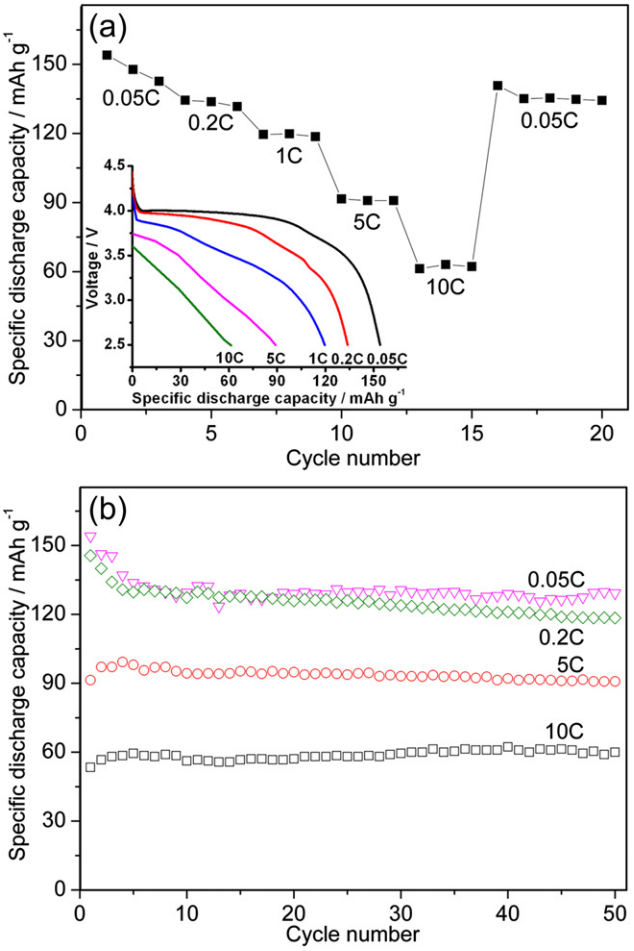

Fig. 7. (a) Rate capabilities and (b) cycling performances of C-LiMnPO$_4$ synthesized at the optimized conditions.

The cycling performances of C-LiMnPO$_4$ at various discharge rates are presented in Fig. 7b. Fairly good cycling stabilities are exhibited at low discharge rates. The capacity retentions at 0.05C and 0.2C from the 6th to the 50th cycle are 97.7% and 90.5%, respectively. Excellent cycling behaviors are observed at the high rates of 5C and 10C. No capacity fades are found over 50 cycles, demonstrating that the electrochemical process is quite reversible at high rates. The capacity loss at low discharge rates such as 0.05C and 0.2C may be due to the side reaction between active material and electrolyte [13,33].

4. Conclusions

In this work, the C-$LiMnPO_4$ nanocomposite with high electrochemical performance is successfully synthesized by an acetate-assisted antisolvent precipitation method combined with ball milling and heat treatment. The nanosize of the precursor is controlled by high supersaturation in the precipitation process, which is induced by acetate and antisolvent. The coated carbon layer suppresses the particle growth in the subsequent heat treatment for the preparation of C-$LiMnPO_4$. The nanosized precursor and coat coating both contribute to the formation of nanoscale C-$LiMnPO_4$ particles. Our C-$LiMnPO_4$ nanocomposite exhibits excellent rate capability and stable cyclability. The proposed synthetic strategy provides a facile and universal method for the preparation of other candidate electrode materials with nanometric particle size and high electrochemical performance.

Acknowledgments

This work was financially supported by the Ministry of Science and Technology of China (2009AA035200) and the National Natural Science Foundation of China (21035005 and 21275013).

Appendix A. Supplementary information

Supplementary information related to this article can be found at http://dx.doi.org/10.1016/j.jpowsour.2013.01.054.

References

[1] J.M. Tarascon, M. Armand, Nature 414 (2001) 359–367.
[2] V. Etacheri, R. Marom, R. Elazari, G. Salitra, D. Aurbach, Energy Environ. Sci. 4 (2011) 3243–3262.
[3] R. Pitchai, V. Thavasi, S.G. Mhaisalkar, S. Ramakrishna, J. Mater. Chem. 21 (2011) 11040–11051.
[4] A.K. Padhi, K.S. Nanjundaswamy, J.B. Goodenough, J. Electrochem. Soc. 144 (1997) 1188–1194.
[5] L.X. Yuan, Z.H. Wang, W.X. Zhang, X.L. Hu, J.T. Chen, Y.H. Huang, J.B. Goodenough, Energy Environ. Sci. 4 (2011) 269–284.
[6] D. Jugović, D. Uskoković, J. Power Sources 190 (2009) 538–544.
[7] A. Yamada, S.C. Chung, K. Hinokuma, J. Electrochem. Soc. 148 (2001) A224–A229.
[8] M.M. Saidi, H. Huang, Alkali–iron–cobalt Phosphates and Related Electrode Active Material, US Patent No. 7422823, 2008.
[9] C. Delacourt, L. Laffont, R. Bouchet, C. Wurm, J.B. Leriche, M. Morcrette, J.M. Tarascon, C. Masquelier, J. Electrochem. Soc. 152 (2005) A913–A921.
[10] S.K. Martha, B. Markovsky, J. Grinblat, Y. Gofer, O. Haik, E. Zinigrad, D. Aurbach, T. Drezen, D. Wang, G. Deghenghi, I. Exnar, J. Electrochem. Soc. 156 (2009) A541–A552.
[11] T. Shiratsuchi, S. Okada, T. Doi, J.I. Yamaki, Electrochim. Acta 54 (2009) 3145–3151.
[12] T. Drezen, N.H. Kwon, P. Bowen, I. Teerlinck, M. Isono, I. Exnar, J. Power Sources 174 (2007) 949–953.
[13] T.N.L. Doan, I. Taniguchi, J. Power Sources 196 (2011) 1399–1408.
[14] D.Y. Wang, H. Buqa, M. Crouzet, G. Deghenghi, T. Drezen, I. Exnar, N.H. Kwon, J.H. Miners, L. Poletto, M. Grätzel, J. Power Sources 189 (2009) 624–628.
[15] J.F. Ni, L.J. Gao, J. Power Sources 196 (2011) 6498–6501.
[16] A.V. Murugan, T. Muraliganth, P.J. Ferreira, A. Manthiram, Inorg. Chem. 48 (2009) 946–952.
[17] S.M. Oh, S.W. Oh, C.S. Yoon, B. Scrosati, K. Amine, Y.K. Sun, Adv. Funct. Mater. 20 (2010) 3260–3265.
[18] C. Delacourt, P. Poizot, M. Morcrette, J.M. Tarascon, C. Masquelier, Chem. Mater. 16 (2004) 93–99.
[19] J.L. Liu, D.G. Hu, T. Huang, A.S. Yu, J. Alloys Compd. 518 (2012) 58–62.
[20] T.H. Kim, H.S. Park, M.H. Lee, S.Y. Lee, H.K. Song, J. Power Sources 210 (2012) 1–6.
[21] J. Xiao, W. Xu, D. Choi, J.G. Zhang, J. Electrochem. Soc. 157 (2010) A142–A147.
[22] S.M. Oh, S.T. Myung, Y.S. Choi, K.H. Oh, Y.K. Sun, J. Mater. Chem. 21 (2011) 19368–19374.
[23] S.M. D'Addio, R.K. Prud'homme, Adv. Drug Deliv. Rev. 63 (2011) 417–426.
[24] A.A. Thorat, S.V. Dalvi, Chem. Eng. J. 181–182 (2012) 1–34.
[25] H. Zhao, J.X. Wang, Q.A. Wang, J.F. Chen, J. Yun, Ind. Eng. Chem. Res. 46 (2007) 8229–8235.
[26] J. Zhong, Z.G. Shen, Y. Yang, J.F. Chen, Int. J. Pharm. 301 (2005) 286–293.
[27] K.F. Hsu, S.Y. Tsay, B.J. Hwang, J. Mater. Chem. 14 (2004) 2690–2695.
[28] G. Meligrana, C. Gerbaldi, A. Tuel, S. Bodoardo, N. Penazzi, J. Power Sources 160 (2006) 516–522.
[29] G. Hasegawa, Y. Ishihara, K. Kanamori, K. Miyazaki, Y. Yamada, K. Nakanishi, T. Abe, Chem. Mater. 23 (2011) 5208–5216.
[30] Y.D. Cho, G.T.K. Fey, H.M. Kao, J. Power Sources 189 (2009) 256–262.
[31] D. Choi, D.H. Wang, I.T. Bae, J. Xiao, Z.M. Nie, W. Wang, V.V. Viswanathan, Y.J. Lee, J.G. Zhang, G.L. Graff, Z.G. Yang, J. Liu, Nano Lett. 10 (2010) 2799–2805.
[32] H.C. Yoo, M.K. Jo, B.S. Jin, H.S. Kim, J. Cho, Adv. Energy Mater. 1 (2011) 347–351.
[33] F. Wang, J. Yang, P.F. Gao, Y. NuLi, J.L. Wang, J. Power Sources 196 (2011) 10258–10262.